Energy 202 (2020) 117727

Contents lists available at ScienceDirect

Energy

journal homepage: www.elsevier.com/locate/energy

Energy analysis and techno-economic assessment of a hybrid PV/HKT/BAT system using biomass gasifier: Cuenca-Ecuador case study

Antonio Cano [a], Paul Arévalo [a, b], Francisco Jurado [a, *]

[a] Department of Electrical Engineering, University of Jaen, Spain
[b] Department of Electrical Engineering, University of Cuenca, Ecuador

ARTICLE INFO

Article history:
Received 13 January 2020
Received in revised form
21 March 2020
Accepted 26 April 2020
Available online 30 April 2020

Keywords:
Gasifier biomass
Hybrid autonomous grid
Energy control
Sensitivity analysis
Modelling

ABSTRACT

This paper analyzes the impact on an off-grid renewable hybrid system composed of photovoltaic energy, hydrokinetic turbines, batteries and biomass gasifiers, using various types of biomass in order to determine the optimal configuration of the system located in southern Ecuador. Three types of energy dispatch, charge cycle, load following and combined cycle have been proposed with the objective of determining new patterns on the behavior of sources with respect to electric demand.

The biomass used as an energy resource produces electricity through a biomass gasifier that feeds a microturbine. Considering the types of biomass consumed by the gasifier, the items such as net present cost and cost of energy have been analyzed for the different types of control. Sensitivity studies indicate the increase in the cost of the system by increasing the minimum state of charge in the batteries. However, this increase reduces biomass consumption and CO_2 emissions. Finally, the variation of the cost in the components influences the total cost of the system, being the fuel and the photovoltaic system the systems that have the highest sensitivity, the results have shown that the renewable system is able to supply the demand without violating any norm.

1. Introduction

Hybrid systems complement each other to overcome the variable nature of renewable energy sources, which together with the energy storage system (ESS), can improve system reliability and energy sustainability. The integration of small distributed energy sources, such as biomass gasifiers (GB), hydrokinetic turbines (HKT), batteries (BT), and photovoltaic (PV) is a trend that is currently being developed.

There are different software for the optimization of hybrid systems, such as HOMER [1,2] and iHOGA [3], they have been used by different authors to optimize the design of hybrid systems, articles [4,5] study mainly indicators such as the NPC, the COE, the unmet load and the CO_2 emissions. Developed different methodologies to optimize hybrid systems were presented in Ref. [6].

Downdraft gasifiers have been studied in Ref. [7] to drive gas or MT engines and produce electricity. The authors [8] carried out a review, with the two main typologies of small-scale gasifiers (fixed and fluidized bed), and the document [9] presented an electricity generator model that integrates a gasifier and a 200 kW gas turbine to analyze the feasibility of using solid biomass as fuel. In this regard, a study of the design and performance improvements of the gasifiers was developed in Ref. [10].

Some authors have studied the different types of biomass that feed downdraft gasifiers, paper [11] analyzed the use of cobs in the gasification process. Corncobs have been tested in an 18-kW downdraft gasifier for power generation using different resistive loads (4, 8, and 12 kW) and cold gas efficiency varied in the range of 33.7%–37.0%. In Refs. [12] An experimental investigation of a downdraft biomass gasifier is carried out using furniture wood and wood chips under various operating conditions, and the cold gas efficiency of the biomass gasifier is found to be of the order of about 80% whereas the overall efficiency of the biomass electrical power producing system is of the order of 10–11%. The authors [13,14] performed a thermodynamic analysis of a gasifier with different types of biomass. There are software packages to model the behavior of gasifiers. A program was developed to predict the performance in Ref. [15]. In this regard, a thermodynamic model was described [16]. Based on Cycle-Tempo software, a combined investigation of experimentation and modeling in an integrated gasifier-motor-generator system was presented in Ref. [17], the

* Corresponding author.
E-mail address: fjurado@ujaen.es (F. Jurado).

https://doi.org/10.1016/j.energy.2020.117727
0360-5442/

Abbreviations

P_{PV}	Photovoltaic output power [kW]
Y_{PV}	Nominal capacity of the photovoltaic generator [kW]
f_{PV}	Reduction factor of the photovoltaic generator [%]
I_T	Incident radiation in the photovoltaic module [kW/m^2]
I_s	Solar incident radiation under standard test conditions [kW/m^2]
α_P	Temperature coefficient of the photovoltaic module [%/°C]
T_C	PV cell temperature [°C]
T_S	PV cell temperature under standard operating conditions [°C]
η_g	Gasifier efficiency [%]
Q_g	Volumetric gas flow inside the gasifier [Nm^3/h]
LHV_b	Lower Heating Value of the Biomass [kJ/kg]
LHV_g	Lower Heating Value of the gas [MJ/kg]
M_b	Rate of biomass consumption [kg/h]
P_{MTg}	Estimated power generated by the gasifier - microturbine MT [kW]
HHV_g	High Heating Value of the Biomass [MJ/kg]
η_{MT}	Efficiency of microturbine (MT) [%]
P_{bg}	Nominal electrical power generated by the MT-gasifier system [kW]
η_{gen}	Efficiency of the electric generator connected to the microturbine (MT) [kW]
η_{el}	Electrical performance of the gasifier-MT system [%]
P_{aux}	Power required by the gasifier-MT equipment [kW]
P_{in}	Real output power of the gasifier system - MT [kW]
E_{bg}	Annual gasifier production [kWh]
CUF	Gasifier utilization factor [%]
P_{HKT}	Hydrokinetic turbine output power [kW]
E_{HKT}	Hydrokinetic turbine output energy [kW]
ρ_w	Water density [kg/m^3]
$C_{p,H}$	Performance coefficient of the hydrokinetic turbine [%]
η_{HKT}	Combined efficiency of the electric generator and hydrokinetic turbine [%]
A	Swept area of the hydrokinetic turbine [m^2]
v	Water speed [m/s]
t	Time [s]
$SOC(t)$	State of charge batteries in time t
$P_{bat}(t)$	Battery power output [kW]
V_{bus}	Voltage in bus [V]
η_{bat}	Battery efficiency [%]
SOC_{min}	Minimum state of charge in batteries [%]
C_n	Nominal capacity of the battery bank [Ah]
C_b	Nominal capacity of each battery [Ah]
N_{bat}	Total number of batteries
T_{bat}^{life}	Period of time in batteries since the beginning of the year [h]
$Life_{HS}$	Life expectancy of the hybrid system [year]
$Life^{pu,year}$	Battery life in the last year [year]
$Ceil$	Maximum near limit of the expression as a whole batteries
$P_0(t)$	Inverter output power [kW]
$P_i(t)$	Inverter input power [kW]
η_{inv}	Inverter efficiency [%]
P_{inv}	Nominal power of the inverter [kW]
C_{acap}	Capital and installation costs [$]
C_R	Replacement costs [$]
C_f	Fuel costs [$]
$C_{O\&M}$	Annual cost of operation and maintenance [$]
NPC	Net Present Cost [$]
COE	Cost of Energy [$/kWh]
TAC	Total annual cost of the system [$]
CRF	Cost of capital recovery [$]
n	Years of project life [year]
i	Annual interest rate [%]
$Q(l)$	Diesel consumption [l]
D_f	Distance further from the origin of the biomass [km]
Qt_c	Diesel consumption in a standard truck [l/km]
$C_t(USD)$	Transportation cost of biomass [$]
$C_{O\&M}$	Cost of operation and maintenance in transport trucks [$]
$C_m(USD)$	Truck maintenance cost according to your route [$]
C_{tb}	Cost of biomass transported to the plant [$/ton]
F_0	Gasifier interception coefficient [units/h/kW]
F_1	Gasifier fuel slope [units/h/kW]
P_{load}	Load power [kW]

integrated model has standard deviations lower than 10% when predicting syngas composition and cold gas efficiency. The largest standard deviation when predicting waste heat is 12.81%, for redwood pellets and woodchips, the highest cold gas efficiency/power generation efficiency is 75.0%/16.4% and 80.8%/19.0%, respectively. The article [18] presents an experimental and analytical study on a rural house heating system using solar energy and biomass, experimental tests have indicated that the energy efficiency and primary exergy are 67.66% and 16.17% respectively, demonstrating their viability with experimental data [19]. The PV system alone cannot supply the load, it needs another support system [20].

The optimal sizing of hybrid systems with biogas and biomass was developed to supply the electricity demand [21,22]. As well as, biomass gasifiers and photovoltaic panels in hybrid systems have been analyzed by some authors to satisfy the load profiles [23–27]. Likewise, a hybrid system composed of photovoltaic energy and biomass is capable of providing electricity at a cheaper cost than its independent parts, the system was simulated in Homer software [28]. In Ref. [29] the authors modeled and optimized the off-grid hybrid energy system using Homer pro and Matlab (genetic algorithm) using solar and biomass energy. The results have shown that the genetic algorithm has less cost of energy and unmet load with respect to Homer pro with greater penetration of the photovoltaic generator and less CO_2 emissions [29]. Another experimental study, it refers to the gasification process of non-woody biomass, such as straw or corn. The effects of the operating conditions on the gasification performance in terms of the gasifier temperature profiles were investigated. According to the experimental results, the operating conditions have a great influence on the gasifier temperature profiles and the distribution of the Product gas composition and gasification efficiency resulted in 73.61% [30].

This paper presents a novel study related to the optimization of an autonomous hybrid system composed of PV/HKT/BT/GB, to determine behavior patterns under several configurations. This study analyzes some types of biomass existing in the southern of Ecuador (Cuenca) to produce electricity through a GB that feeds a MT microturbine. Three energy control strategies have been discussed using the Homer pro computational tool to improve the reliability of the system. The GB feeds the load in the absence of a renewable source (solar and hydrokinetic). The photovoltaic

component in laboratory shown in Photography 1. The nominal capacity of 35 kWp consisting of 140 photovoltaic solar panels of 250 Wp each, brand Atersa (Spain), distributed as follows: 60 fixed panels oriented at an angle of 5° north of monocrystalline type with 15 kW capacity; 60 fixed panels oriented at an angle of 5° north polycrystalline type 15 kW capacity [31].

Photography 1. Photovoltaic system in the laboratory.

The smart hydro hydrokinetic turbine in the laboratory has 5 kW of power, shown in Photography 2 [31].

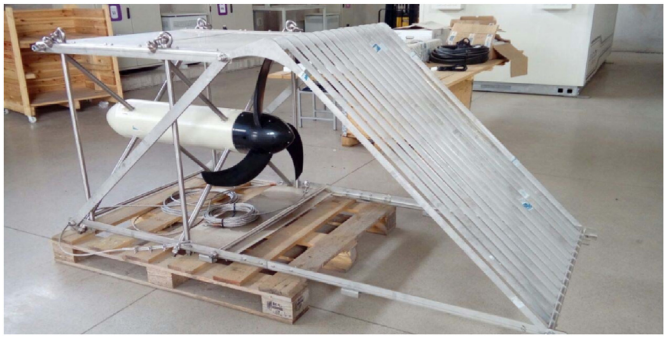

Photography 2. Hydrokinetic turbine in the laboratory.

The biomass gasifier system is shown in Photography.3. The project RESOLIVE, used a 70 kWe and 110 kWth downdraft gasifier and gas-powered engine.

Photography 3. Downdraft gasifier 70 kWe.

This document has been organized as follows: in section 2, the load demand curve is indicated and mathematical models are raised. Section 3 describes the cost analysis of the system components. In section 4, the proposed energy dispatch control schemes are presented and sensitivity analysis, making a comparison and discussion of the results obtained in section 5. Section 6 presents a comparison with similar studies. Finally, section 7 presents the conclusions.

2. Hybrid system model

The hybrid system used in this paper consists of a PV, HKT, GB connected to a MT and an energy storage system using BAT (lead acid). Fig. 1 shows the hybrid system used.

2.1. Case study

The case study is a University located in southern Ecuador (2°48′13.0″S 78°52′00.5″W), the demand curve is presented in Fig. 2. The daily demand data has been taken from the energy meters of the University, so they are real data.

It is clear that peak demand occurs at night with 30 kW and the minimum demand occurs at dawn with 10 kW on average. The average hourly radiation for one year is shown in Fig. 3. The real solar radiation data has been taken from the meteorological station installed at the University (study load).

The radiation is relatively constant during the year, due to the location of the study site. In addition to the solar resource, there is a water resource close to the demand, the average hourly speed for a year of the river is shown in Fig. 4. The river speed data has been calculated from real flow data for a year, these data have been taken from a hydrological station located on the Burgay river, which is located near the load under study.

Four types of biomass have been proposed, depending on their availability and distance from the source, the average monthly consumption for one year is shown in Fig. 5.

The resource of each type of biomass has been obtained from real data taken in each production sector, through surveys in factories and distributors.

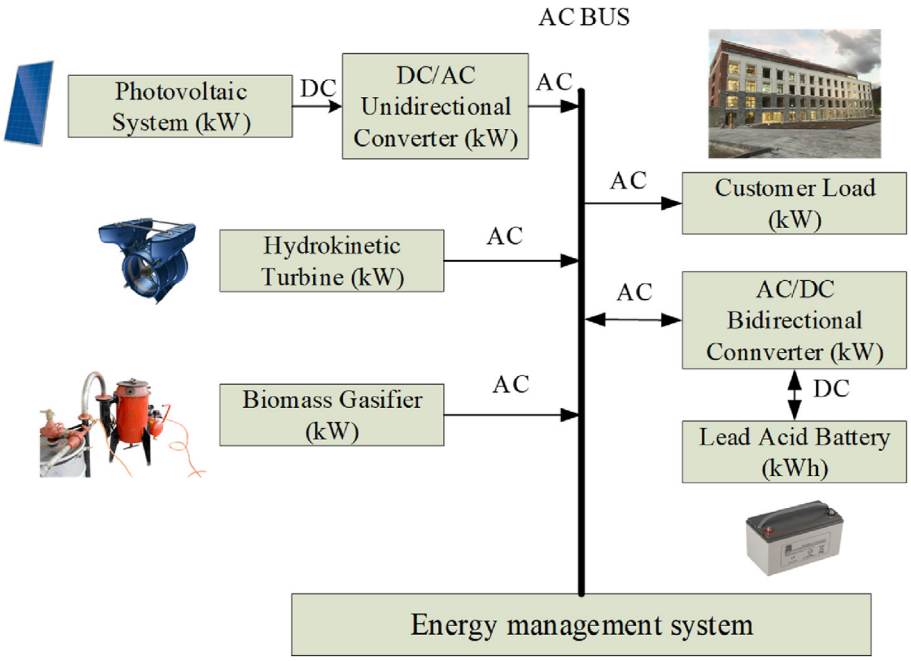

Fig. 1. Proposed hybrid system.

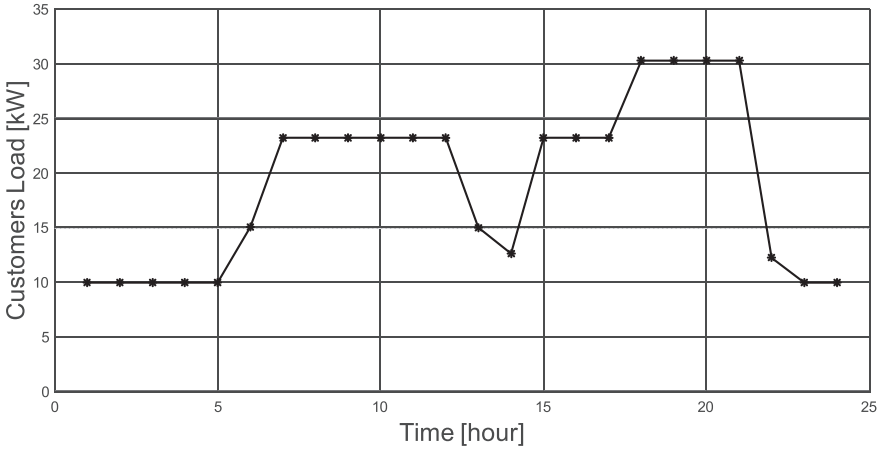

Fig. 2. Daily load demand [kW].

2.2. Photovoltaic model

The performance of a solar module changes according to the climatic conditions of the installation site. The photovoltaic power varies regarding to the solar radiation incident in the module and the environmental factors (ambient temperature, humidity, etc.). The power of the P_{PV} system is calculated using Eq. (1) [32].

$$P_{PV} = Y_{PV} \times f_{PV}\left(\frac{I_T}{I_S}\right)[1 + \alpha_P \times (T_C - T_S)] \quad (1)$$

2.3. Model of gasifier biomass

In biomass gasification technology, solid bio-wastes are transformed, forming a gaseous fuel that is finally used for electricity generation. In the case of the biomass gasifier, the gas produced is used as an input fuel to the MT. Studies have shown that the efficiency of the primary energy of biomass is 16.67% [18].

The purpose of the biomass gasification system is to generate energy by the combustible gases obtained from the total process. The performance of the gasifier η_g is given by Eq. (3) [14–17,30]:

$$\eta_g = \frac{Q_g \times LHV_g}{\dot{m}_b \times LHV_b} \times 100 \quad (3)$$

The estimated power generated is calculated with the following Eq. (4) [33].

$$P_{MTg} = \frac{\text{Total gas} \times HHV_g \times \eta_{MT}}{365} \quad (4)$$

MT efficiency around 30%. The gas produced includes the gases produced in pyrolysis, tar reforming and coal gasification processes. The efficiency of microturbine is given by:

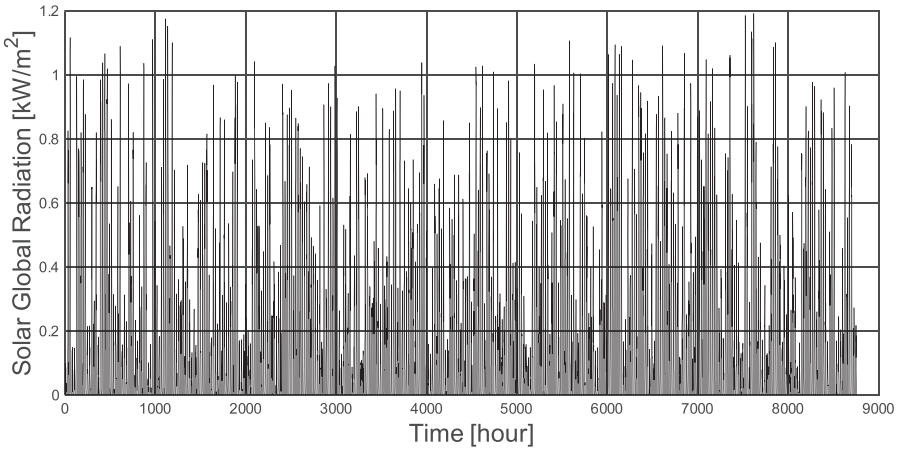

Fig. 3. Global solar radiation [kW/m^2].

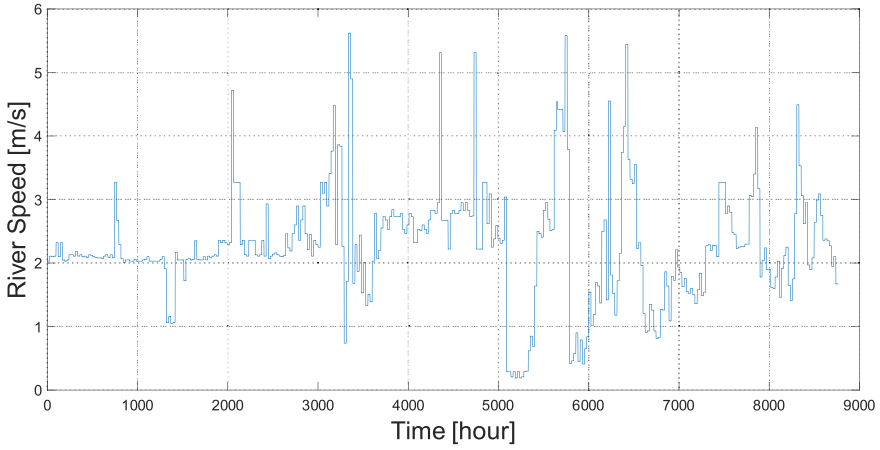

Fig. 4. River speed [m/s].

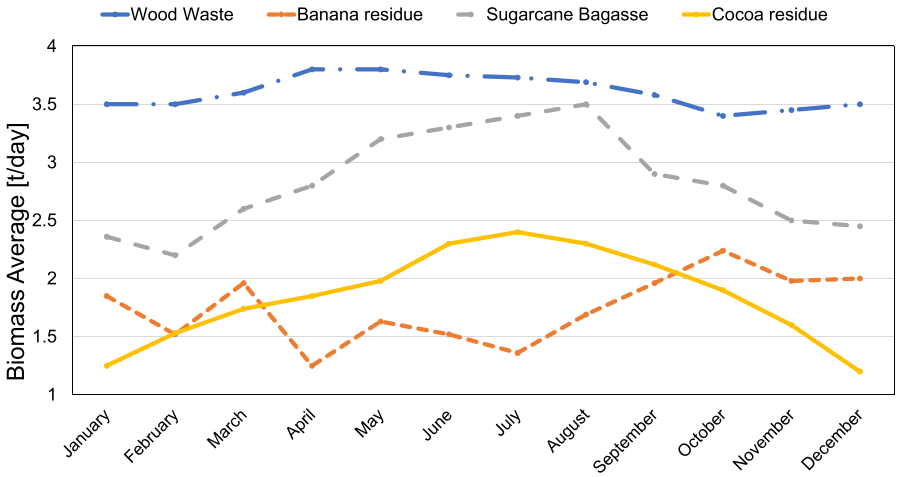

Fig. 5. Average biomass consumption [t/day].

$$\eta_{MT} = \frac{P_{bg}}{(\dot{m}_b \times LHV_g) \times \eta_{gen}} \times 100 \quad (5)$$

Generator efficiency is close to 95%. The electrical efficiency is given by Eq. (6) [34]:

$$\eta_{el} = \eta_g \times \eta_{MT} \times \eta_{gen} \quad (6)$$

The electrical performance of the gasifier-MT system is given by Ref. [8]:

$$\eta_{el} = \frac{P_{in} - P_{aux}}{(Input\ biomass)_{LHV}} = \frac{P_{bg}}{(Input\ biomass)_{LHV}} \quad (7)$$

The annual production of electricity E_{bg} from a biomass gasifier can be calculated as,

$$E_{bg} = P_{bg} \times (8760 \times CUF) \quad (8)$$

2.4. Model of hydrokinetic turbines

The characteristics of the HKT depend on the river speed. In this study, a hydrokinetic turbine of 5 kW is used. The feasibility of using hydrokinetic turbines (HKT) in off-grid systems has been proposed in Ref. [4]. The electrical output power of HKT is given by Eq. (9) [35].

$$P_{HKT} = \frac{1}{2} \cdot \rho w \cdot A \cdot v^3 \cdot C_{p,H} \cdot \eta_{HKT} \quad (9)$$

where the energy is given by:

$$E_{HKT} = P_{HKT} \times t \quad (10)$$

2.5. Model of energy storage system

The batteries are used as a system to store excess energy or to discharge when the energy that comes from renewable sources is insufficient. Energy measurement can be achieved with the proper estimation of the state of charge (SOC). The SOC of the battery is a function of time and can be calculated as,

$$SOC(t) = SOC(t-1) \int_{t-1}^{t} \frac{P_b(t) \times \eta_{bat}}{V_{bus}} dt \quad (11)$$

To calculate the number of N_{bat} batteries during the operation of the hybrid system life, the following Eq. (12) is used:

$$N_{bat} = \text{ceil}\left(\frac{Life_{HS} \times Life_{bat}^{pu.year}}{T_{bat}^{life}}\right) \quad (12)$$

2.6. Inverter model

The inverter is used to connect the DC bus to the AC current, using Eq. (13). Determine the power of the load side.

$$P_0(t) = P_i(t)\eta_{inv} \quad (13)$$

The efficiency of the inverter is 96%. The input power of the P_{inv} inverter will be given by the PV power and battery power.

3. Economic analysis

In this study, the Net Present Cost (NPC) of the proposed hybrid system is minimized, while maintaining the optimal energy flow. For an optimal configuration, four main factors are determined: the number of PV, BT, HKT and nominal capacity of GB.

For the economic analysis, the concept of the annual cost of the system (TAC) is used [36].

$$TAC = C_{acap} + \sum_{i=1}^{n} C_{O\&M,i} + C_f + \sum_{i=1}^{n} C_{R,i} \quad (14)$$

The cost of energy (COE) (€/kWh), defined as the average cost of one kWh of energy, is calculated as follows:

$$\text{COE}(€/\text{kWh}) = \frac{NPC(€)}{\sum_{h=1}^{h=8760} P_{load}(h)(kWh)} \times \text{CRF} \quad (15)$$

The NPC represents the cost of the system life cycle, the present value of all installation and operation costs throughout the life of the project.

$$\text{NPC} = \frac{TAC}{CFR(i,n)} \quad (16)$$

where CRF can be calculated by:

$$\text{CRF}(i,n) = \frac{i(1+i)^n}{(1+i)^n - 1} \quad (17)$$

The cost details of each component of the renewable hybrid system (HRES) are presented in Table 1.

To perform the simulation in Homer, it is essential to identify several parameters such as those shown in Table 2. The simulation will determine the optimal value.

Diesel consumption Q_d in (l) is calculated with the following Eq. (18):

$$Q_d = D_f \times Qt_d \quad (18)$$

Therefore, the average cost of transporting biomass C_t ($) is:

$$C_t = Q_d \times C_d \quad (19)$$

Additionally, according to Table 2, the cost of transport includes a cost per operation and maintenance $C_{o\&m}$ and D_f is the farthest transport distance of biomass in (km) of 0.5 ($/km), so the maintenance cost C_m ($) is:

$$C_m = D_f \times \text{C}_{\text{o\&m}} \quad (20)$$

The cost per ton of transported biomass C_{tb} ($) is given by Eq. (25) and is shown in Table 3.

$$C_{tb} = C_t + C_m \quad (21)$$

Since the place of study is located in southern Ecuador, the maximum transport distance of each biomass in the surrounding area has been detailed.

It is necessary to determine the parameters of the gasifier since for each biomass proposed, the interception coefficients (F_0) and the fuel slope (F_1) will be different in each case, Table 4 shows the characteristics of each type of biomass and the calculated parameters.

Table 1
Characteristic of the system components.

System	Capital Cost ($/kW)	Replacement ($/kW)	O&M ($/year)
Gasifier [37]	781.25	325	0.065 $/op.h
PV [38]	1300	500	10
HKT [4,35,39]	1900	1060	50
BAT/acid lead [32,39,40]	300	150	10
Converter [39]	300	300	0

Table 2
Average cost of heavy load transportation.

Parameters	Values
Average fuel consumption (l/km) [41,42]	0.1746
Diesel cost (USD/l) [43]	0.27
Vehicles O&M cost (USD/km) [43]	0.5

4. Control strategies

In this system, the GB remains at the lowest priority, that is, it works only when PV, HKT and BAT are unable to meet the load demand. The steps of the operational strategy are as follows:

4.1. Cycle charging control

In the control of the charging cycle, the priority of the system is to recharge the batteries with the gasifier at maximum power when conditions arise. The operation of the algorithm is explained below in Fig. 6:

i. If the total energy produced by PV and HKT is sufficient and SOC(t) < SOC_{min}(t). The demand is supplied by renewable and the battery is charged with the GB at maximum power.

$$P_{load}(t) = P_{HKT}(t) + \frac{P_{PV}(t)}{\eta_{inv}} \quad (22)$$

$$P_{bat}\ (t) = P_{GBmax}\ (t) \quad (23)$$

ii. If the total energy produced by PV and HKT is sufficient and SOC(t) ≥ SOC_{min}(t). There is excess energy that must be deferred.

ii. In the case that the energy generated by PV and HKT is insufficient and the batteries SOC(t) < SOC_{min}(t), then the energy to meet the load demand is supplied by GB at maximum power.

$$P_{load}(t) = P_{GBmax}(t) \quad (24)$$

The excess energy will serve to recharge the batteries

$$P_{bat}(t) = P_{GBmax}(t) - P_{load}(t) \quad (25)$$

iv. In the case that the energy generated by PV and HKT is insufficient and the batteries SOC(t) ≥ SOC_{min}(t), then the energy to meet the load demand is supplied by renewable sources and batteries.

4.2. Load following control

Unlike the CC control, the LF control has as a priority to supply the load with the GB according to the power that the demand requires.

i. First, the LF strategy. If the total energy produced by PV and HKT is sufficient and SOC(t) < SOC_{min}(t). The demand is supplied by renewable sources.

$$P_{load}(t) = P_{HKT}(t) + \frac{P_{PV}(t)}{\eta_{inv}} \quad (26)$$

The excess renewable sources energy will serve to recharge the batteries

Table 3
Calculation of the cost of transport of biomass at the study site.

Fuel	Scaled annual average (t/day)	Furthest distance (km)	Diesel consumption (l)	Transport cost (USD)	Additional costs (USD)	Total ($/t)
Banana residue	1.75	120	20,952	5,65704	60	65,65704
Cocoa residue	1.85	110	19,206	5,18562	55	60,18562
Cane Bagasse residue	2.83	60	10,476	2,82852	30	32,82852
Wood Residue	3.61	40	6984	1,88568	20	21,88568

Table 4
Characteristic of the type of biomass used.

Parameter	Wood residue	Banana residue	Cane Bagasse residue	Cocoa residue
LHV biomass (MJ/kg) [44]	19	12,63	19,85	6464
Carbon content (%) [38,45,46]	4,96	41,6	29	5,24
Scaled annual average (t/d) [45]	3,61	1,75	2,83	1,85
Average price ($/t)	21,88	65,65	32,82	60,18
F_0	0,0001	0,00013	0,0002	0,0043
F_1	1,5788	2375	1513	4,64

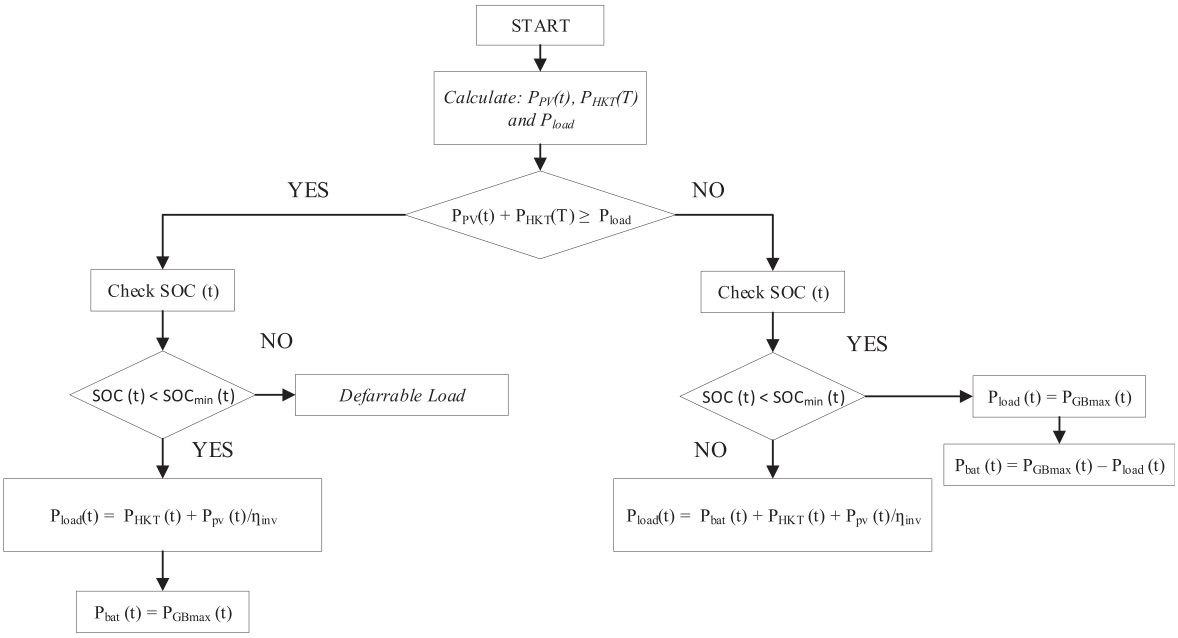

Fig. 6. Flow chart CC control.

$$P_{bat} = P_{HKT}(t) + \frac{P_{PV}(t)}{\eta_{inv}} - P_{load}(t) \quad (27)$$

ii. If the total energy produced by PV and HKT is sufficient and SOC(t) $\geq$ SOC_{min}(t). There is excess energy that must be deferred.

ii. In the case that the energy generated by PV and HKT is insufficient and the batteries SOC(t) < SOC_{min}(t), then the energy to meet the load demand is supplied by GB according to the power that the demand requires.

$$P_{GB}(t) = P_{load}(t) \quad (28)$$

iv. In the case that the energy generated by PV and HKT is insufficient and the batteries SOC(t) $\geq$ SOC_{min}(t), then the energy to meet the load demand is supplied by renewable sources and batteries.

$$P_{load}(t) = P_{bat}(t) + P_{HKT}(t) + \frac{P_{PV}(t)}{\eta_{inv}} \quad (29)$$

In the third strategy CD. The decision of the controller depends on the cost of energy production. Depending on the system conditions, you must choose between CC and LF. Because the load and conditions are random, the dispatch strategy uses the current net charge (renewable charge-energy) to make a decision. The controller must use the CC strategy (Fig. 6) if the current net charge is low (approximately less than 50%). On the other hand, if the current net load is high, the controller must select the LF strategy (Fig. 7). Homer optimizes each of the options to meet the demand by comparing the cost of charging the battery with the DG with the cost of charging the battery using excess renewable energy.

5. Results

Table 5 shows the result of the optimization. Firstly, the GB and HKT components for all cases are kept at a constant power (18 kW and 4 units respectively). Therefore, the variables are: photovoltaic energy, battery capacity and biomass consumption.

The objective variable in this case is greenhouse gas emissions, which depend on the amount of biomass burned per year, fuel (t/year), when using the LF control it is evident that the amount of fuel used is less with respect to a CC and CD, therefore CO and NOx emissions are lower with the cocoa residue with minimum values followed by the wood residue. To use a smaller quantity of biomass, the photovoltaic power must be greater as well as the capacity of the batteries. However, they do not represent higher levels of emissions.

Fig. 8 shows the energy control strategies taken from a random sample of 100 h per year; In Fig. 8 the batteries accumulate more energy, causing the GB to shut down during future periods of low charge by demonstrating the DC control presented in Fig. 6. In Fig. 9, the LF control has been brought to out, generating electrical energy according to the load required and not recharging the batteries as in DC, demonstrating the algorithm presented in Fig. 7.

The CD uses the net present load to avoid future problems, with the purpose of deciding whether the batteries should be recharged using the GB or excess power, so it uses the CC dispatch when the net load is low and LF when it is high. This strategy ensures the continuous operation of the GB, the CD is shown in Fig. 10, the state of charge of the batteries has a different performance from the previous ones since the gasifier has the priority of supplying energy.

On the other hand, Fig. 11 shown the optimal NPC ($) using different types of biomass, the wood residue under CC control is the most economical with an NPC of $ 247,686 and a COE of 0.182 $/kWh shown in Fig. 12. In addition, CO_2 emissions are lower (Fig. 13) and excess energy (Fig. 14), since under CC control the system charging the batteries and not supplying the load directly, also depends on the availability and characteristics of the biomass type.

In Fig. 15 the electrical production of each energy source is shown, the penetration of the GB is lower under the LF control because it supplies the demand only with the required power.

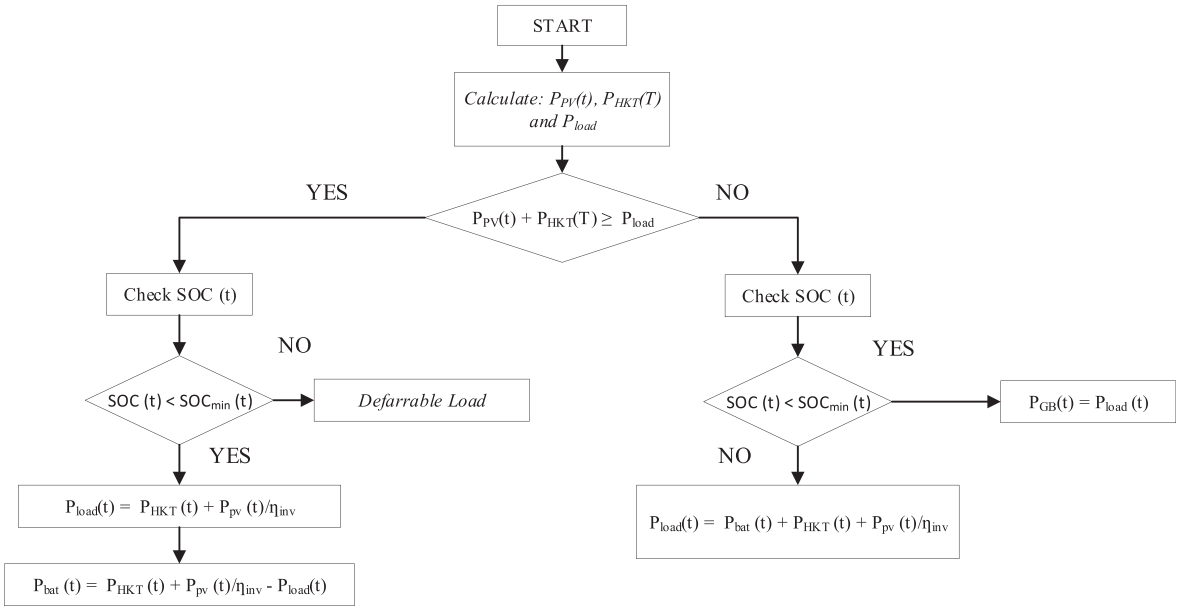

Fig. 7. Flow chart LF control.

Table 5
HRES system optimization.

Parameters	Wood residue			Banana residue			Cane bagasse residue			Cocoa residue		
	CC	LF	CD	CC	LF	CD	CC	LF	CD	CC	LF	CD
Loss of power supply probability (%)	0.06	0.06	0	0.04	0.04	0	0.06	0.07	0	0.04	0.07	0
CO emissions (kg/yr)	0.2	0.12	0.29	0.29	0.09	0.43	0.19	0.11	0.27	0.54	0.04	0.84
NOx emissions (kg/yr)	0.13	0.07	0.18	0.18	0.06	0.27	0.12	0.07	0.17	0.34	0.03	0.52
Gasifier												
Capacity (kW)	18	18	18	18	18	18	18	18	18	18	18	18
Fuel (t/year)	102	28.2	142	145	46	214	97.4	52.5	136	271	20.1	419
PV												
Capacity (kW)	20.6	79	124	28.2	242	125	20.6	84.9	124	35	452	124
BAT												
Capacity (kWh)	120	320	236	112	328	228	120	340	236	124	292	240
Autonomy (h)	5.92	15.8	11.6	5.53	16.2	11.3	5.92	16.8	11.6	6.14	14.4	11.8
Converter												
Capacity (kW)	27.7	45.2	42.3	19.7	18	49.6	27.7	68.3	42.3	21	30	45.5
HKT												
Quantity	4	4	0	4	4	0	4	4	0	4	4	0

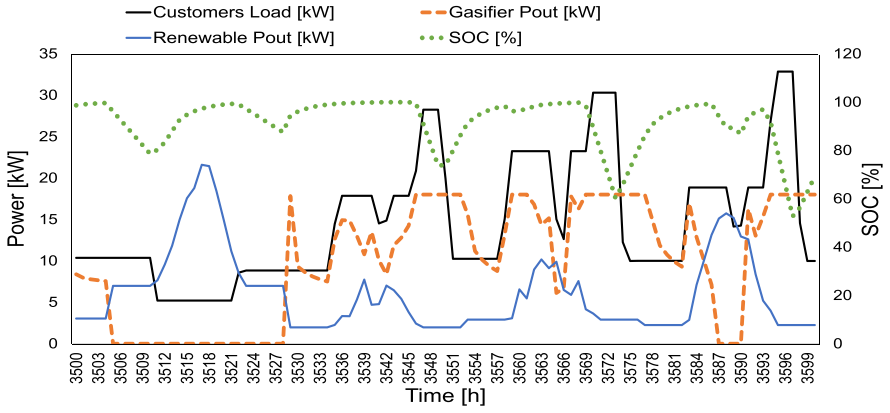

Fig. 8. Result of the energy control strategies under CC control.

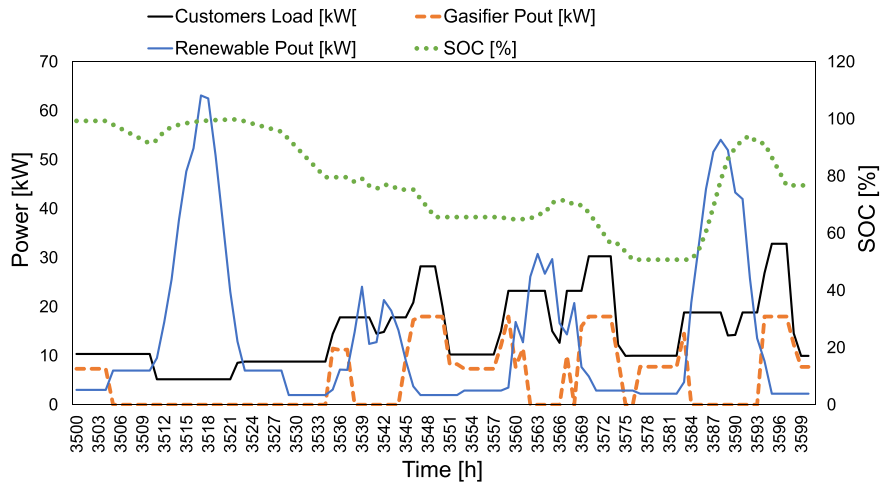

Fig. 9. Result of the energy control strategies under LF control.

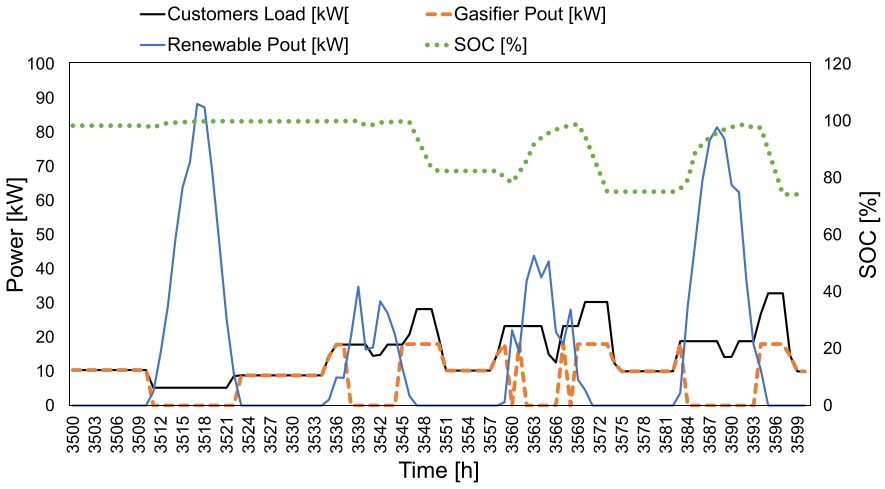

Fig. 10. Result of the energy control strategies under CD control.

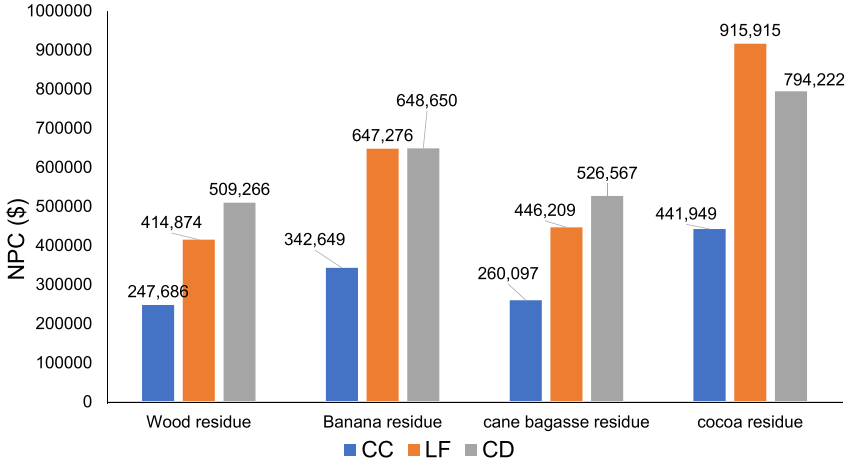

Fig. 11. Economic optimization result of the hybrid system (NPC).

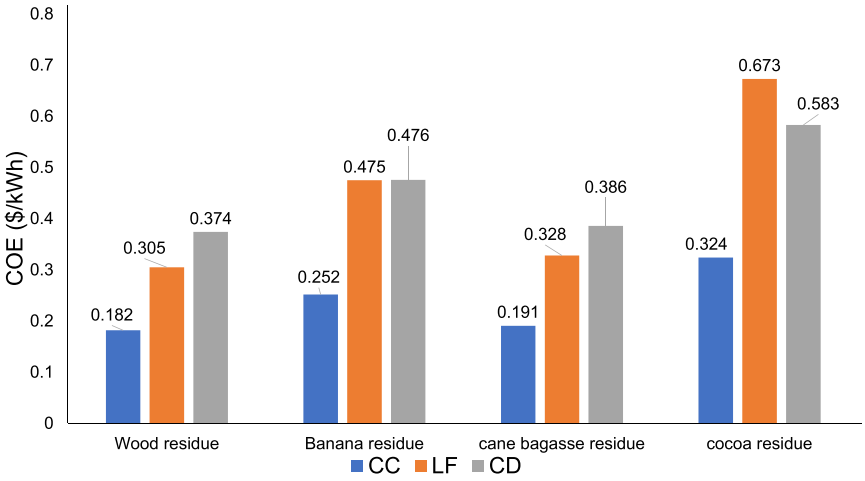

Fig. 12. Economic optimization result of the hybrid system (COE).

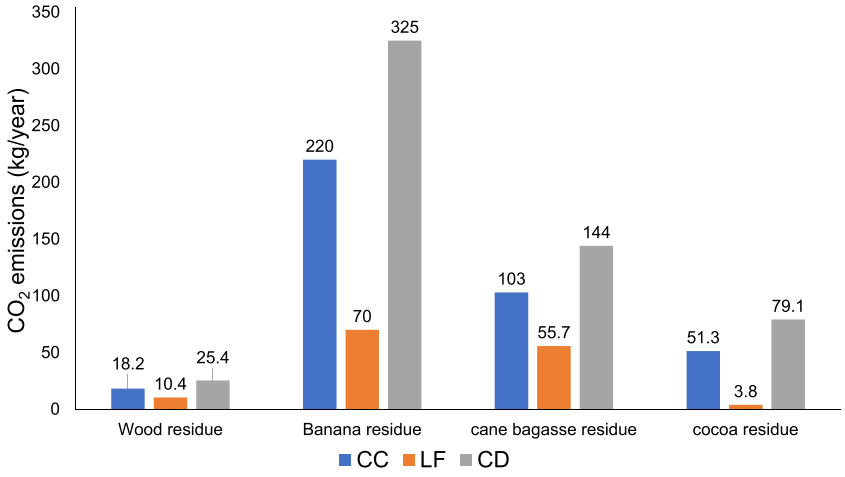

Fig. 13. Environmental optimization result of the hybrid system.

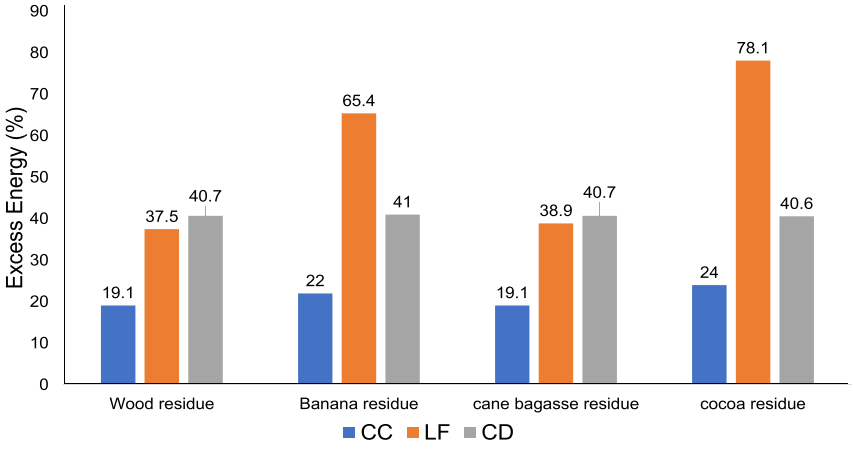

Fig. 14. Energy optimization result of the hybrid system.

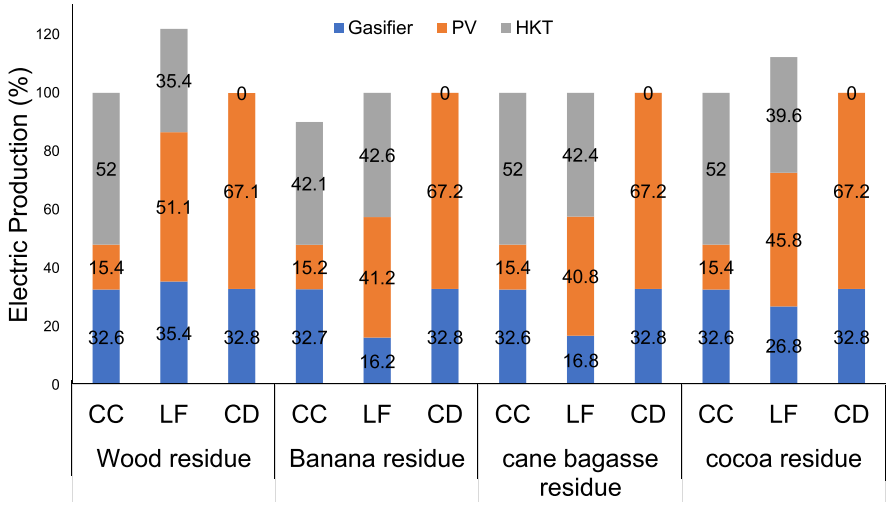

Fig. 15. Electricity production with different types of biomass.

However, the PV power is greater than CC and DC. The CC control chooses more HKT power due to its low price, increasing the penetration of the GB to recharge the batteries, the CD control chooses higher PV by increasing the price of energy, these results coincide with the data obtained in Table 5.

A sensitivity analysis of the SOC_{min} with respect to cost and fuel consumption was performed. Fig. 16 (a) shows an increase in cost while SOC_{min} is higher The DC control, which takes priority to recharge the batteries, presents a low-cost increase when the SOC_{min} is higher. Therefore, the system would use less energy to recharge the batteries. The LF control, if it has less capacity in the batteries (higher SOC_{min}), would have to use more GB, which would further increase the cost of the system. CD control is a combination of CC and LF. The results are shown in Fig. 16 (a) and Fig. 16 (b).

Regarding the consumption of biomass (kg/year), and CO_2 emissions (kg/year), it is evident that, for a larger SOC_{min}, there will be a lower performance of the GB, so biomass consumption and CO_2 emissions it will be relatively lower, as shown in Fig. 16 (b).

Fig. 17 (a) shows the variation of the Time step with respect to the NPC ($) and COE ($/kWh). While, if the resolution is increased

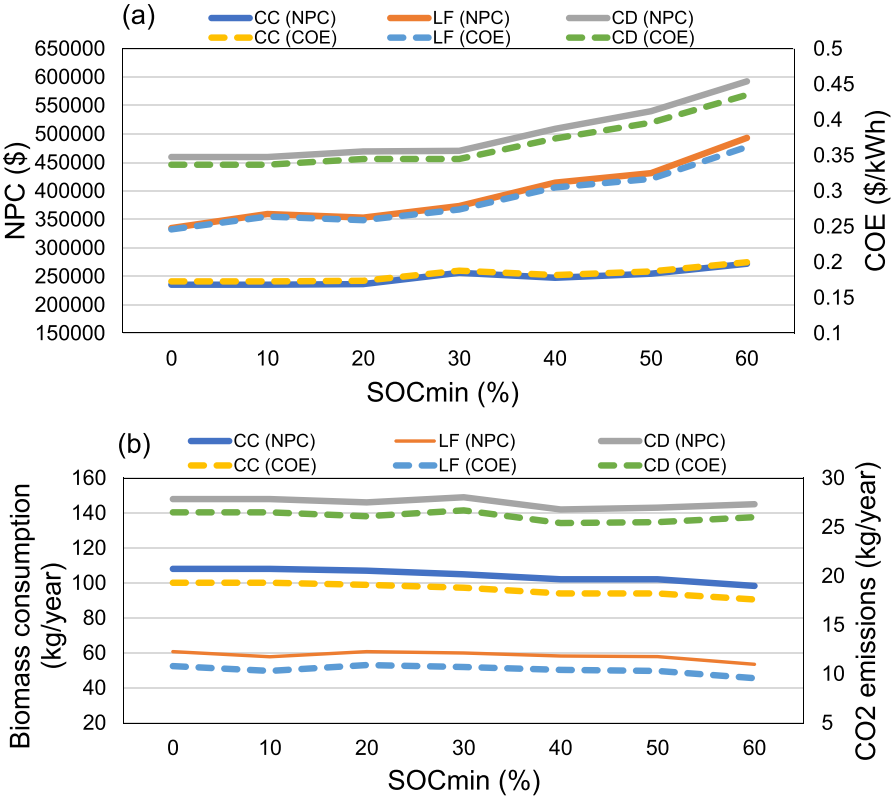

Fig. 16. SOC_{min} sensitivity analysis (wood).

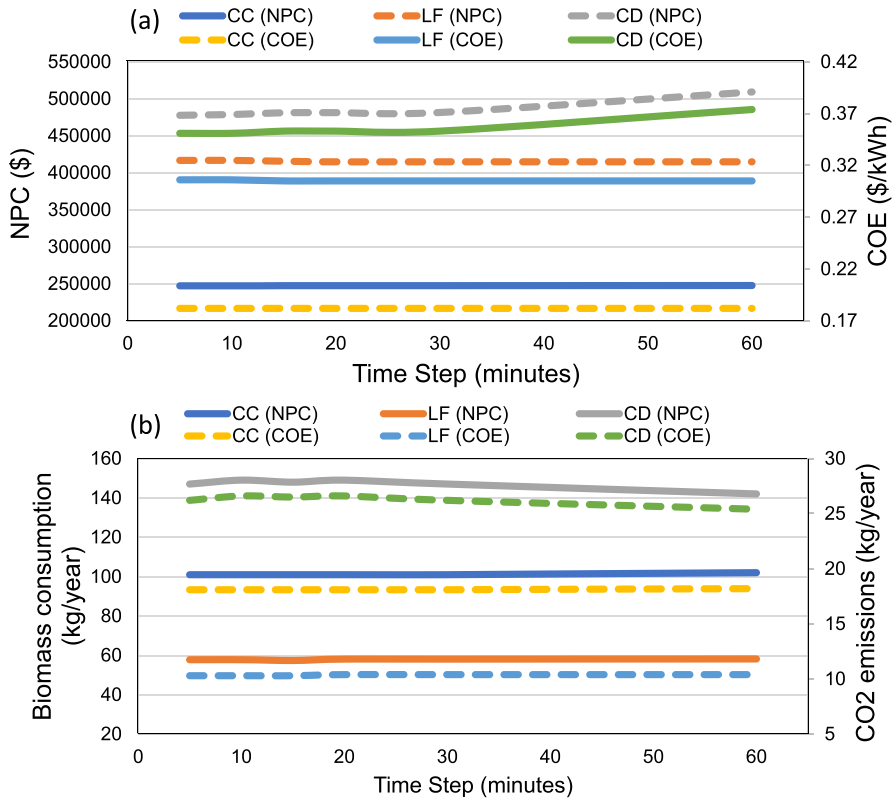

Fig. 17. Sensitivity analysis. Time step (wood).

the cost of the system is slightly lower, so it is recommended to perform the analysis with samples in an interval of 5 min. The same behavior has shown the consumption of biomass (kg/year) and CO_2 emissions (kg/year) in Fig. 17 (b).

Because the cost of the components is variable with respect to time, a sensitivity analysis of the variation in the cost of capital has

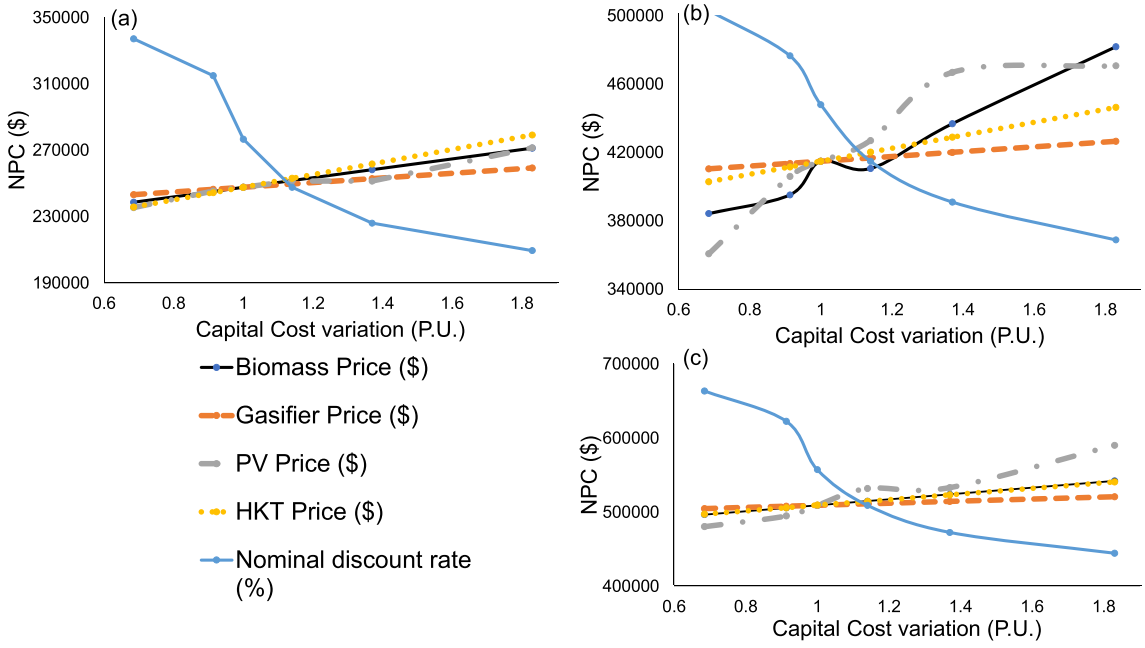

Fig. 18. Sensitivity analysis, variation of the cost of capital with respect to NPC. (a) CC (b) LF (c) CD.

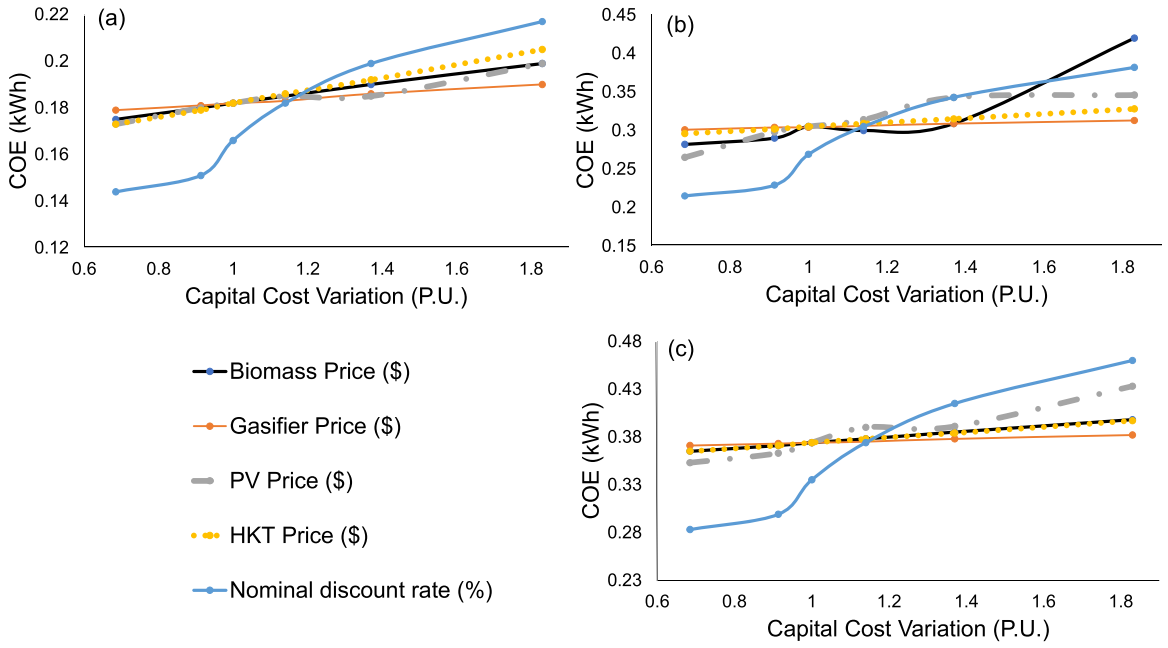

Fig. 19. Sensitivity analysis variation of the cost of capital with respect to COE. (a) CC (b) LF (c) CD.

been performed in some indices with respect to NPC and COE.

In Fig. 18, increasing the cost of capital also increases the NPC under the three energy controls, the price of biomass and PV are the ones that differ in CC and LF due to the control algorithm used, while the nominal discount rate decreases in all cases. From the economic viewpoint, CC control is recommended.

The component which has presented the highest sensitivity is HKT and the lowest is the GB. In this case, there is an increase in the nominal discount rate, under the control LF, Fig. 19 (b), the price of GB does not imply a considerable change in the COE. However, the price of biomass and PV changes its value considerably. Finally, in Fig. 19 (c) it shows a pattern similar to the CC control, with the difference that in this case the HKT component presents a smaller variation and the slightly larger PV component. The results are similar to the study [28] when using the CC control. The variation of the discount rate reflects intervals where the price of electricity is affordable under different scenarios, as in Ref. [47]. In addition, the installation of distributed solar panels avoids losses in the system.

6. Comparison with similar research

There are few studies that make the comparison of an isolated renewable system made up of PV/HKT/BAT/GB; but in some similar studies new results have been found. The comparison is not accurate due to the difference in the size of the systems.

The results of the studies mentioned in Table 6 show different COEs due to the different potencies of each source. However, when comparing with the current study, the values are similar and depending on the subsidies of each country, the cost will change.

7. Conclusions

The results obtained in the analysis of technical-economic optimization of a renewable hybrid system composed of PV/HKT/GB/BAT in an area south of Ecuador, show that for the different types of biomass in the gasifier, there is slight variation of the interception parameters and fuel slope.

Table 6
Comparison with other studies.

Ref.	Country	Hybrid Renewable System				COE ($/kWh)	Dispatch Method
		Source 1 (kW)	Source 2 (kW)	Source 3 (kW)	Source 4 (kW)		
[28]	India	PV (13.7)	Biomass (14.2)	Diesel (26.5)	–	0.27	CC
					–	0.2	GA
[29]	India	PV (100)	FC (57)	Wind (50)	Biomass (50)	0.214	CC
					Biomass (50)	0.163	GA
[47]	Iran	PV (15)	Biogas (10)	DG (10)	Grid (–)	0.193	CC
[20]	Thailand	PV (12.285)	Syngas (13.8)	BAT (60.9)	–	0.2	CC
[25]	Bangladesh	PV (106)	Biomass (55)	DG (40)	–	0.21	CC
[48]	Pakistan	Wind (15,000)	Biogas (20,000)	PV (15,000)	Grid (–)	0.0525	CC
[49]	India	PV (60)	Biogas (6)	DG (10)	BAT (70)	0.197	CC
[24]	India	PV (55)	Biomass (35)	–	BAT (20)	0.12	LF
[23]	India	PV (5)	Biomass (5)	FC (5)	BAT	0.13	CC
Present Study	Ecuador	PV (20.06)	HKT (20)	Biomass (Wood) (18)	BAT (120)	0.118	CC
						0.305	LF
						0.374	CD

The highest production occurs with the combined control with 67.2% with banana residues, cane bagasse residue and cocoa residues, while under the LF control the highest PV penetration is presented by the system with wood residue, with 51.1%, while the CC control is more equitable with a slightly higher percentage of HKT, with 52% HKT penetration with systems using wood, cane bagasse and cocoa residues. In addition, wood waste has been found to have the lowest NPC and COE with $ 247,686 and $ 0.182/kWh under CC control, this is due to the low cost, and availability of this type of biomass.

Similarly, sensitivity studies have shown that the PV/HKT/GB/BAT system fueled by wood waste has an increase in NPC and COE if the SOC_{min} of the batteries increases, The greatest increase has been presented by the LF control, the NPC has increased by $ 170,000 and the COE by $ 0.17/kWh. Hence, the consumption of biomass (kg/year) and CO_2 emissions (kg/year) decrease slightly with 10 kg/year under the CC control, the LF and CD controls show less variations between 8 kg/year and 5 kg/year respectively. A similar behavior resulted from the sensitivity analysis with respect to (Time step) for the CD control, whereas under the CC and LF controls the values are constant. Under CD control, the shorter the sampling interval (5 min), the cost increases (NPC increases by $ 30,000 and COE increases by $ 0.02/kWh. In addition, biomass consumption and CO_2 emissions decrease in 5 kg/year and 3 kg/year respectively.

The variation in the capital cost implies an increase in the NPC and COE of the system. In this case, the increase in the price of biomass and photovoltaic generators, are those that have generated the greatest increase in the NPC and the COE under the CD, with an increase in NPC of $ 90,000 and $ 130,000 respectively, and the increase of COE is 0.15 $/kWh for the biomass price and 0.08 $/kWh for the PV system.

The NPC of the GB and HKT, in most cases under CC control, have increased by $ 3000 and $ 4000 and the COE has increased by 0.01 $/kWh and 0.02 $/kWh respectively. In addition, the variation in the nominal discount rate has been more representative under CD control, with a decrease in the NPC of $ 2000 and an increase in COE of $ 0.17/kWh.

The results have shown that it is feasible from the technical-economic point of view, to provide an off-grid load by means of a system formed by PV/HKT/GB/BAT. Therefore, the possibility of adding an additional source or an alternative storage system is promising, which will be developed in future work.

References

[1] HOMER's Calculations [Online]. Available: https://www.homerenergy.com/products/pro/docs/latest/homers_calculations.html. [Accessed 18 March 2020].

[2] HOMER pro - microgrid software for designing optimized hybrid microgrids [Online]. Available: https://www.homerenergy.com/products/pro/index.html. [Accessed 18 March 2020].

[3] iHOGA – simulation and optimization of stand-alone and grid-connected hybrid renewable systems [Online]. Available: https://ihoga.unizar.es/en/. [Accessed 18 March 2020].

[4] Cordero PA, Benavides DJ, Jurado F. Energy control and sizing optimization of an off grid hybrid system (wind-hydrokinetic-diesel). In: 4th IEEE Colombian conference on automatic control: automatic control as key support of industrial productivity. CCAC; 2019. https://doi.org/10.1109/CCAC.2019.8921056. 2019 - Proceedings.

[5] Cano A, Jurado F, Sánchez H, Fernández LM, Castañeda M. Optimal sizing of stand-alone hybrid systems based on PV/WT/FC by using several methodologies. J Energy Inst Nov. 2014;87(4):330–40. https://doi.org/10.1016/j.joei.2014.03.028.

[6] Castañeda M, Cano A, Jurado F, Sánchez H, Fernández LM. Sizing optimization, dynamic modeling and energy management strategies of a stand-alone PV/hydrogen/battery-based hybrid system. Int J Hydrogen Energy Apr. 2013;38(10):3830–45. https://doi.org/10.1016/j.ijhydene.2013.01.080.

[7] Muthu Dinesh Kumar R, Anand R. "Production of biofuel from biomass downdraft gasification and its applications," *Advanced Biofuels*. Elsevier; 2019. p. 129–51.

[8] Bocci E, Sisinni M, Moneti M, Vecchione L, Di Carlo A, Villarini M. State of art of small scale biomass gasification power systems: a review of the different typologies. Energy Procedia 2014;45:247–56. https://doi.org/10.1016/j.egypro.2014.01.027.

[9] Henao NC, Lora EES, Maya DMY, Venturini OJ, Franco EHM. "Technical feasibility study of 200 kW gas microturbine coupled to a dual fluidized bed gasifier. Biomass Bioenergy 2019;130:105369. https://doi.org/10.1016/j.biombioe.2019.105369. Nov.

[10] Susastriawan AAP, Saptoadi H, Purnomo. Small-scale downdraft gasifiers for biomass gasification: a review. Renewable and sustainable energy reviews, vol. 76. Elsevier Ltd; 01-Sep. p. 989–1003. https://doi.org/10.1016/j.rser.2017.03.112.

[11] Martínez LV, Rubiano JE, Figueredo M, Gómez MF. Experimental study on the performance of gasification of corncobs in a downdraft fixed bed gasifier at various conditions. Renew Energy Apr. 2020;148:1216–26. https://doi.org/10.1016/j.renene.2019.10.034.

[12] Zainal ZA, Rifau A, Quadir GA, Seetharamu KN. Experimental investigation of a downdraft biomass gasifier. Biomass Bioenergy Oct. 2002;23(4):283–9. https://doi.org/10.1016/S0961-9534(02)00059-4.

[13] Jaén RL, Recio ÁR, Preston T, Rodríguez LQ, Ruiz LO. "Análisis termodinámico de un gasificador 'Ankur' modelo WBG-10 trabajando con diferentes biomasas. Revista Tecnología Química 2008;XXVIII(No. 2).

[14] Antonopoulos IS, Karagiannidis A, Gkouletsos A, Perkoulidis G. Modelling of a downdraft gasifier fed by agricultural residues. Waste Manag Apr. 2012;32(4):710–8. https://doi.org/10.1016/j.wasman.2011.12.015.

[15] Sharma AK. Modeling and simulation of a downdraft biomass gasifier 1. Model development and validation. Energy Convers Manag Feb. 2011;52(2):1386–96. https://doi.org/10.1016/j.enconman.2010.10.001.

[16] Fortunato B, Brunetti G, Camporeale SM, Torresi M, Fornarelli F. Thermodynamic model of a downdraft gasifier. Energy Convers Manag 2017;140:281–94. https://doi.org/10.1016/j.enconman.2017.02.061.

[17] Li CY, Shen Y, Wu JY, Dai YJ, Wang CH. "Experimental and modeling investigation of an integrated biomass gasifier–engine–generator system for power generation and waste heat recovery. Energy Convers Manag 2019;199:112023. https://doi.org/10.1016/j.enconman.2019.112023. Nov.

[18] Zhang X, et al. Experimental and analytic study of a hybrid solar/biomass rural heating system. Energy Jan. 2020;190:116392. https://doi.org/10.1016/j.energy.2019.116392.

[19] Pérez-Navarro A, et al. Experimental verification of hybrid renewable systems as feasible energy sources. Renew Energy Feb. 2016;86:384–91. https://doi.org/10.1016/j.renene.2015.08.030.

[20] Kohsri S, Meechai A, Prapainainar C, Narataruksa P, Hunpinyo P, Sin G. Design and preliminary operation of a hybrid syngas/solar PV/battery power system for off-grid applications: a case study in Thailand. Chem Eng Res Des Mar. 2018;131:346–61. https://doi.org/10.1016/j.cherd.2018.01.003.

[21] Chauhan A, Saini RP. Techno-economic optimization based approach for energy management of a stand-alone integrated renewable energy system for remote areas of India. Energy Jan. 2016;94:138–56. https://doi.org/10.1016/j.energy.2015.10.136.

[22] Goel S, Sharma R. "Optimal sizing of a biomass–biogas hybrid system for sustainable power supply to a commercial agricultural farm in northern Odisha, India. Environ Dev Sustain Oct. 2019;21(5):2297–319. https://doi.org/10.1007/s10668-018-0135-x.

[23] Singh A, Baredar P. Techno-economic assessment of a solar PV, fuel cell, and biomass gasifier hybrid energy system. Energy Rep Nov. 2016;2:254–60. https://doi.org/10.1016/j.egyr.2016.10.001.

[24] Rajbongshi R, Borgohain D, Mahapatra S. Optimization of PV-biomass-diesel and grid base hybrid energy systems for rural electrification by using HOMER. Energy May 2017;126:461–74. https://doi.org/10.1016/j.energy.2017.03.056.

[25] Islam MS, Akhter R, Rahman MA. A thorough investigation on hybrid application of biomass gasifier and PV resources to meet energy needs for a northern rural off-grid region of Bangladesh: a potential solution to replicate in rural off-grid areas or not? Energy Feb. 2018;145:338–55. https://doi.org/10.1016/j.energy.2017.12.125.

[26] Palatel A. Biomass gasifier integrated hybrid systems as a sustainable option for rural electrification. In *green Energy and technology*, no. 9789811083921. Springer Verlag; 2018. p. 257–70.

[27] Singh M, Balachandra P. "Microhybrid electricity system for energy access, livelihoods, and empowerment," *proc.* IEEE Sep. 2019;107(9):1995–2007. https://doi.org/10.1109/JPROC.2019.2910834.

[28] Chambon CL, Karia T, Sandwell P, Hallett JP. Techno-economic assessment of biomass gasification-based mini-grids for productive energy applications: the case of rural India. Renew Energy Jul. 2020;154:432–44. https://doi.org/10.1016/j.renene.2020.03.002.

[29] Suresh V, Muralidhar M, Kiranmayi R. Modelling and optimization of an off-grid hybrid renewable energy system for electrification in a rural areas. Energy Rep Nov. 2020;6:594–604. https://doi.org/10.1016/j.egyr.2020.01.013.

[30] Gai C, Dong Y. Experimental study on non-woody biomass gasification in a downdraft gasifier. Int J Hydrogen Energy Mar. 2012;37(6):4935–44. https://doi.org/10.1016/j.ijhydene.2011.12.031.

[31] Espinoza JL, Gonzalez LG, Sempertegui R. "Micro grid laboratory as a tool for research on non-conventional energy sources in Ecuador," in *2017*. IEEE International Autumn Meeting on Power, Electronics and Computing, ROPEC 2017, 2018;2018-January:1–7. https://doi.org/10.1109/ROPEC.2017.8261615.

[32] Das BK, Al-Abdeli YM, Woolridge M. Effects of battery technology and load

scalability on stand-alone PV/ICE hybrid micro-grid system performance. Energy Feb. 2019;168:57–69. https://doi.org/10.1016/j.energy.2018.11.033.
[33] Situmorang YA, Zhao Z, Yoshida A, Kasai Y, Abudula A, Guan G. Potential power generation on a small-scale separated-type biomass gasification system. Energy Jul. 2019;179:19–29. https://doi.org/10.1016/j.energy.2019.04.163.
[34] Lee U, Balu E, Chung JN. An experimental evaluation of an integrated biomass gasification and power generation system for distributed power applications. Appl Energy Jan. 2013;101:699–708. https://doi.org/10.1016/j.apenergy.2012.07.036.
[35] Lata-García J, Jurado F, Fernández-Ramírez LM, Sánchez-Sainz H. Optimal hydrokinetic turbine location and techno-economic analysis of a hybrid system based on photovoltaic/hydrokinetic/hydrogen/battery. Energy Sep. 2018;159:611–20. https://doi.org/10.1016/j.energy.2018.06.183.
[36] Haghighat Mamaghani A, Avella Escandon SA, Najafi B, Shirazi A, Rinaldi F. Techno-economic feasibility of photovoltaic, wind, diesel and hybrid electrification systems for off-grid rural electrification in Colombia. Renew Energy Nov. 2016;97:293–305. https://doi.org/10.1016/j.renene.2016.05.086.
[37] Ankur scientific energy technologies pvt. Ltd. [Online]. Available: https://www.ankurscientific.com/ankur-gasifiers-biomass-Combo.html. [Accessed 19 March 2020].
[38] Cortés Martínez R, Lobelles-Sardiñas GO, López-Bastida EJ. Propuesta de mejora tecnológica en la recuperación de azufre de la refinería de petróleo de Cienfuegos. Tecnol. Química 2019;39(1):160–82.
[39] Arévalo P, Benavides D, Lata-García J, Jurado F. Energy control and size optimization of a hybrid system (photovoltaic-hidrokinetic) using various storage technologies. Sustainable cities and society, vol. 52. Elsevier Ltd; 01-Jan. p. 101773. https://doi.org/10.1016/j.scs.2019.101773.
[40] Acevedo-Arenas CY, et al. MPC for optimal dispatch of an AC-linked hybrid PV/wind/biomass/H2 system incorporating demand response. Energy Convers Manag Apr. 2019;186:241–57. https://doi.org/10.1016/j.enconman.2019.02.044.
[41] Cifras agroproductivas [Online]. Available: http://sipa.agricultura.gob.ec/index.php/cifras-agroproductivas. [Accessed 19 March 2020].
[42] Estado de uso de la biomasa para la producción de bioenergía, biocombustibles y bioproductos en Ecuador [Online]. Available: https://www.researchgate.net/publication/286756139_Estado_de_uso_de_la_biomasa_para_la_produccion_de_bioenergia_biocombustibles_y_bioproductos_en_Ecuador. [Accessed 19 March 2020].
[43] Ecuador precios del diesel, 16-marzo-2020 | GlobalPetrolPrices.com. [Online]. Available: https://es.globalpetrolprices.com/Ecuador/diesel_prices/. [Accessed 19 March 2020].
[44] Atlas bioenergético del Ecuador. INP; 2014.
[45] Obtencion de Biocarbon | biomasa | energía renovable [Online]. Available: https://es.scribd.com/document/401944918/Obtencion-de-Biocarbon. [Accessed 19 March 2020].
[46] Abril González MF. Optimización de la reacción de hidrólisis ácida de los residuos de la planta de banano, para mayor rendimiento a glucosa. 2016.
[47] Kasaeian A, Rahdan P, Rad MAV, Yan WM. Optimal design and technical analysis of a grid-connected hybrid photovoltaic/diesel/biogas under different economic conditions: a case study. Energy Convers Manag Oct. 2019;198:111810. https://doi.org/10.1016/j.enconman.2019.111810.
[48] Ahmad J, et al. Techno economic analysis of a wind-photovoltaic-biomass hybrid renewable energy system for rural electrification: a case study of Kallar Kahar. Energy Apr. 2018;148:208–34. https://doi.org/10.1016/j.energy.2018.01.133.
[49] Bhatt A, Sharma MP, Saini RP. Feasibility and sensitivity analysis of an off-grid micro hydro-photovoltaic-biomass and biogas-diesel-battery hybrid energy system for a remote area in Uttarakhand state, India. Renewable and sustainable energy reviews, vol. 61. Elsevier Ltd; 01-Aug. p. 53–69. https://doi.org/10.1016/j.rser.2016.03.030.